Segmentation of transform systems on the East Pacific Rise: Implications for earthquake processes at fast-slipping oceanic transform faults

Patricia M. Gregg Massachusetts Institute of Technology/WHOI Joint Program in Oceanography, Woods Hole, Massachusetts 02543, USA

Jian Lin
Deborah K. Smith
Woods Hole Oceanographic Institution, Woods Hole, Massachusetts 02543, USA

ABSTRACT

Seven of the eight transform systems along the equatorial East Pacific Rise from 12° N to 15° S have undergone extension due to reorientation of plate motions and have been segmented into two or more strike-slip fault strands offset by intratransform spreading centers (ITSCs). Earthquakes recorded along these transform systems both teleseismically and hydroacoustically suggest that segmentation geometry plays an important role in how slip is accommodated at oceanic transforms. Results of thermal calculations suggest that the thickness of the brittle layer of a segmented transform fault could be significantly reduced by the thermal effect of ITSCs. Consequently, the potential rupture area, and thus maximum seismic moment, is decreased. Using Coulomb static stress models, we illustrate that long ITSCs will prohibit static stress interaction between transform segments and limit the maximum possible magnitude of earthquakes on a given transform system. Furthermore, transform earthquakes may have the potential to trigger seismicity on normal faults flanking ITSCs.

Keywords: seismology, earthquake stress triggering, Siqueiros transform fault, transform faults, East Pacific Rise, Clipperton transform fault.

INTRODUCTION

Segmented transform systems are composed of several fault strands offset by short ridges or rifts referred to as intratransform spreading centers (ITSCs) (Menard and Atwater, 1969; Searle, 1983; Pockalny et al., 1997), where active seafloor spreading and crustal accretion are occurring (Fornari et al., 1989; Hekinian et al., 1992; Perfit et al., 1996). Along the equatorial East Pacific Rise between 15° S and 12° N (Fig. 1), the Siqueiros, Quebrada, Discovery, Gofar, Yaquina, Wilkes, and Garrett transform systems have all undergone transtension due to changes in plate motions, and each of these transforms is segmented by at least one ITSC (Searle, 1983; Fornari et al., 1989; Lonsdale, 1989; Goff et al., 1993; Pockalny et al., 1997). The Clipperton transform system has undergone several periods of transpression (Pockalny, 1997), and is the only unsegmented transform system along the equatorial East Pacific Rise.

The global deficiency of seismic moment release on oceanic transform systems has led researchers to hypothesize that a significant portion of oceanic transform slip is accommodated aseismically (e.g., Boettcher and Jordan, 2004). However, global seismicity studies have yet to consider the prevalence of transform fault segmentation. Dziak et al. (1991) observed that earthquake sizes generally correlate with the lengths of individual fault segments at the Blanco transform fault. Our observations of earthquakes recorded on East Pacific Rise transform faults indicate that segmentation is an important factor influencing rupture of large earthquakes at oceanic transforms. While it has been shown that segmentation and fault steps play an important role in controlling the earthquake behavior of continental strike-slip faults (e.g., Harris and Day, 1993), the influence of segmentation and ITSCs on earthquake processes at an oceanic transform system has not been studied in detail.

In this paper, we use teleseismically and hydroacoustically recorded seismicity data from the equatorial East Pacific Rise and Coulomb static stress models to explore the effect of ITSCs on static stress interaction between transform fault segments. We investigate whether adjacent fault segments can behave independently of one another, and how the interaction between segments depends on their offset distance.

TRANSFORM SEGMENTATION

Segmentation of the transtensional transform systems at the equatorial East Pacific Rise has resulted in individual strike-slip fault strands with lengths of 18–89 km, with an average of ~37 km. The ITSCs separating the fault strands have lengths of 5–20 km, with an average length of ~11 km. Fresh lavas collected from the ITSCs within the Siqueiros and Garrett transforms (Hekinian et al., 1992; Perfit et al., 1996) indicate that ITSCs are magmatically active, implying that the regions beneath them are hotter, and thus the lithospheric plate is thinner than the surrounding domains. To explore the effect of segmentation on the transform fault thermal structure, we use a half-space steady-state lithospheric cooling model (McKenzie, 1969; Abercrombie and Ekstrom, 2001). The temperature within the crust and mantle, T, is defined as $T = T_m \mathrm{erf}\,[y(2\kappa t)^{-1/2}]$, where T_m is the mantle temperature at depth, assumed to be 1300 °C; y is the depth; κ is the thermal diffusivity, assumed to be 10^{-6} m^{2}s^{-1}; and t is the age of the lithosphere obtained by dividing distance from the ridge axis by half the spreading rate.

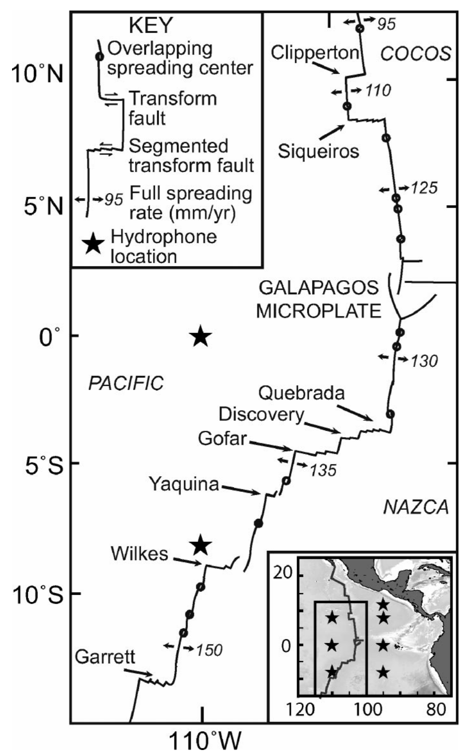

Figure 1. Regional map of the equatorial East Pacific Rise showing large transform and nontransform offsets. Segmentation geometry is included based on previous geological mapping of the transform systems (e.g., Fornari et al., 1989; Lonsdale, 1989). Inset: Regional map showing location of the full array of NOAA Pacific Marine Environmental Laboratory hydrophones.

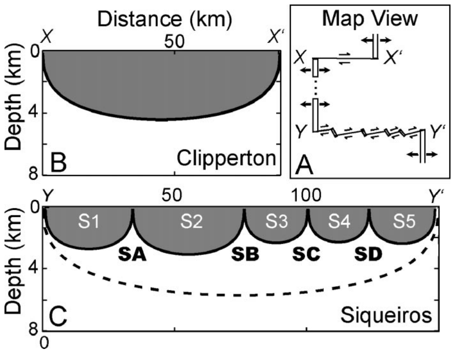

Figure 2. Comparison of estimated areas of brittle lithosphere using a one-dimensional, steady-state lithosphere cooling model (McKenzie, 1969) for the Clipperton (B) and Siqueiros (C) transforms. A: The 90 km Clipperton transform system (X–X′) and the 150 km Siqueiros transform system (Y–Y′), which is broken into five major segments S1, S2, S3, S4, and S5 separated by four ITSCs SA, SB, SC, and SD (Fornari et al., 1989). B: Calculated area of brittle lithosphere for temperatures <600 °C (shaded region) for the Clipperton transform. C: Comparison of the calculated areas of brittle lithosphere for the Siqueiros transform for a model of unsegmented geometry (area above the dotted line) versus a model consisting of five individual segments offset by steady-state ITSCs (shaded area).

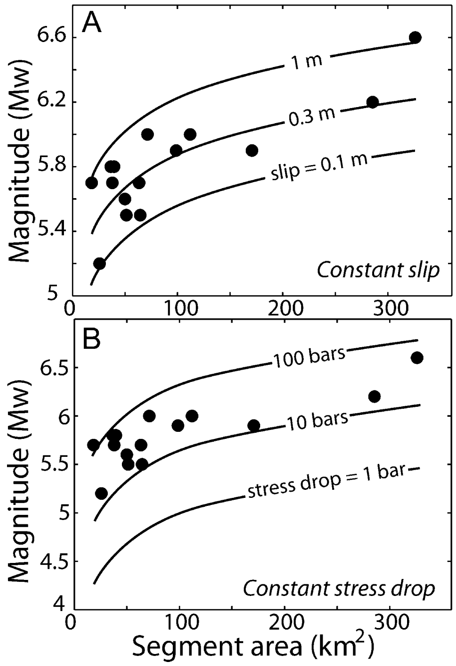

Figure 3. A: The predicted maximum moment magnitude, M_W, of earthquakes (curved lines) for a given transform segment area and a constant slip of 0.1, 0.3, and 1.0 m. The calculations assume that the earthquake ruptures the entire transform segment. Black dots mark the observed maximum M_W recorded on the transform segments of the equatorial East Pacific Rise. The rightmost data point, M_W = 6.6, corresponds to the Clipperton transform. B: The predicted maximum M_W assuming a constant stress drop of transform earthquakes of 1, 10, and 100 bar.

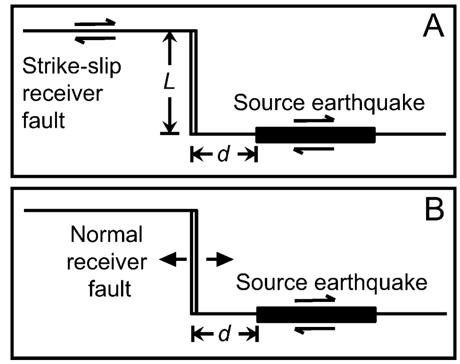

Figure 4. Schematic models showing the geometry of two transform segments bisected by a single ITSC of variable length, *L*. The source earthquake is located on the bottom right transform segment with its left edge located at a distance, *d*, from the ITSC-transform intersection. The source earthquake is assumed to be a strike-slip event on a vertical plane parallel to the transform segment. A: A scenario in which the receiver fault is a strike-slip fault located on the top left transform segment, which is assumed to have the same dip, strike, and rake as the source earthquake. B: A scenario in which the receiver fault is a normal fault located along the ITSC, which is assumed to have a dip of 60° and is parallel to the ITSC.

Figure 2 compares the calculated areas of brittle deformation, defined as regions with calculated temperatures ≤600 °C, for the geometries of the Clipperton and Siqueiros transform systems. The calculated area under the 600 °C isotherm for the Clipperton transform fault is 326 km^2, compared to 710 km^2 for a model of a single unsegmented fault with the cumulative length of the Siqueiros transform system. When the actual segmentation geometry of the Siqueiros transform system is considered, however, the integrated area of the calculated brittle deformation region is decreased by ~60% to 277 km^2.

Seismic moment (M_o), which reflects the energy released by an earthquake, is a function of the rupture area of the fault. Specifically, $M_o = G \times D \times S$, where G is the shear modulus, estimated to be 27 GPa from seismic velocities (Canales et al., 2003), D is the average slip, and S is the estimated brittle area. The resulting moment magnitude is $M_W = (2/3) \times \log(M_o) - 10.73$. For a model of constant stress drop during pure strike-slip earthquakes, $M_o = (\pi/2) \times \Delta\sigma \times w \times S$, where $\Delta\sigma$ is the earthquake stress drop, and w is the fault width, estimated from S divided by fault length (Stein and Wysession, 2003).

Curves in Figure 3 show the predicted earthquake magnitudes for a given fault area, assuming models of constant fault slip (Fig. 3A) or constant stress drop (Fig. 3B) during earthquakes. Earthquakes recorded teleseismically as listed in the Harvard Centroid-Moment Tensor (CMT) catalog were relocated to a specific transform segment using hydroacoustically recorded earthquakes, which have smaller location errors (<6 km) (Fox et al., 2001). The maximum earthquake magnitudes observed on each of the transform fault segments at the equatorial East Pacific Rise from 1996 to 2001 are plotted in Figure 3. Assuming the complete rupture of a given individual fault segment, we can estimate the amount of slip or the stress drop for a given earthquake. For example, the largest earthquake observed on the Clipperton transform has a M_W of 6.6 (Fig. 3). If the entire brittle area of Clipperton (326 km^2) was ruptured during this earthquake, the estimated average slip is 1 m, or the estimated average stress drop is 53 bar or 5.3 MPa.

COULOMB STRESS CALCULATIONS

Evidence for potential earthquake interactions along oceanic transform faults has been noted in several investigations (e.g., Toda and Stein, 2000; Bohnenstiehl et al., 2002, 2004; McGuire et al., 2002; Forsyth et al., 2003). We utilize the methods of King et al. (1994) and Toda et al. (1998) to calculate how static stress from a moderate-sized earthquake is transferred to adjacent faults, and assess the likelihood of rupturing multiple transform segments during a single earthquake. According to Coulomb failure criteria, when an earthquake occurs on a source fault, changes in Coulomb failure stress ($\Delta\sigma_f$) on a receiver fault are expressed as $\Delta\sigma_f = \Delta\tau_s + \mu' \times \Delta\sigma_n$, where $\Delta\tau_s$ and $\Delta\sigma_n$ are changes in shear and normal stresses, on the receiver fault, and μ' is the apparent friction coefficient adjusted for the pore pressure effect (King et al., 1994).

We consider a simple geometry in which two adjacent transform segments are offset by an ITSC of variable length, L, for two scenarios assuming the receiver faults are either strike-slip events along the adjacent transform segment (Fig. 4A) or normal-faulting events located along the ITSC (Fig. 4B). The rupture size for the source earthquake in both cases is varied to reflect typical earthquake magnitudes observed along the segmented transforms of the equatorial East Pacific Rise.

For the first scenario, the calculated maximum change in static stress, $\|\Delta\sigma_f\|$, transferred to the receiver fault is plotted versus L for M_W = 5.0, 5.5, and 6.0 (Fig. 5). As the separation distance between the two transform segments increases, the predicted maximum induced Coulomb stress change on the receiver fault decreases. For example, if $M_w = 6.0$, $d = 0$ km, and L is increased from 5 to 15 km, the calculated $\|\Delta\sigma_f\|$ decreases from 1.35 bar to 0.25 bar (Fig. 5A). The proximity of the earthquake to the ITSC-transform intersection (ITI) is also very important: the closer the source earthquake is located to the ITI (i.e., smaller

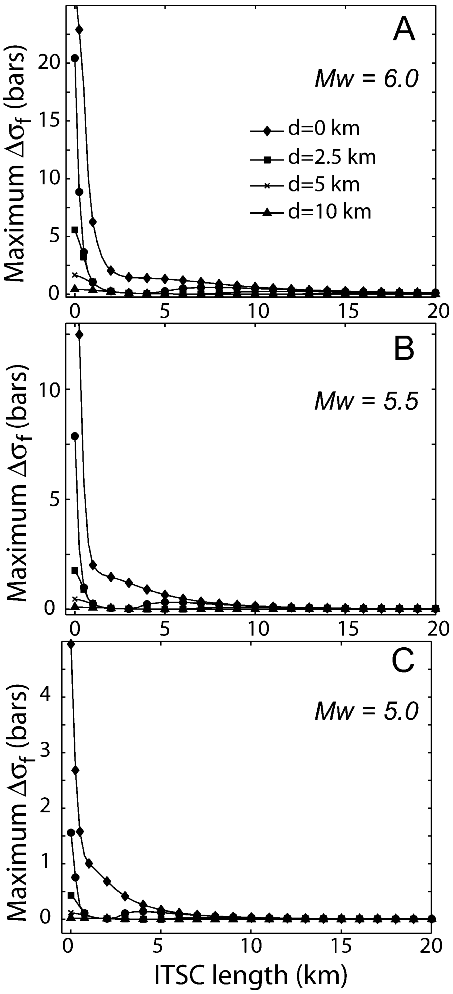

Figure 5. Calculated maximum Coulomb stress changes on a secondary strike-slip receiver fault caused by a strike-slip source earthquake (geometry shown in Fig. 4A) for source earthquake M_w = 6.0, 5.5, and 5.0. Note that the vertical scale is different for each panel. All stress calculations were carried out using a three-dimensional boundary-element model, Coulomb 2.6 (Toda et al., 1998), assuming that both the source and receiver faults extend to a depth of 5 km. For each Coulomb calculation, we used a Young's modulus of 62.5 GPa, a Poisson's ratio of 0.25, an apparent friction coefficient, μ', of 0.4 (e.g., King et al., 1994), and a tapered slip distribution. Stresses are sampled on a horizontal plane at a depth of 2 km. The maximum change in Coulomb stress is taken directly from the point on the receiver fault where Coulomb stress reaches a maximum value. Calculations were carried out for *L* = 1 to 20 km and *d* = 0, 2.5, 5, and 10 km. ITSC—intratransform spreading center.

d), the greater the predicted maximum Coulomb stress change on the receiver fault (Fig. 5). For example, if $M_w = 6.0$, $L = 5$ km, and *d* is increased from 0 to 10 km, the calculated $\|\Delta\sigma_f\|$ decreases from 2.5 bar to 0.1 bar. Previous studies have shown statistically significant correlations between regions of seismicity rate changes following continental strike-slip earthquakes and areas of calculated stress changes >0.2–1.0 bar (Toda et al., 1998).

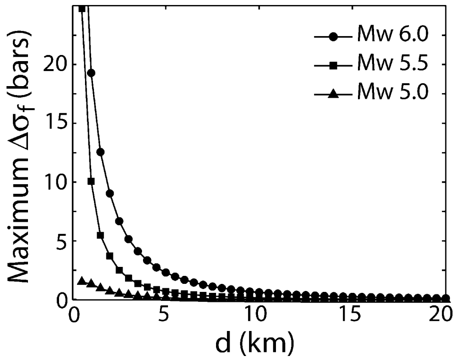

Figure 6. Calculated maximum Coulomb stress changes on a secondary normal receiver fault along the ITSC caused by a strike-slip source earthquake on the adjacent transform segment with geometry shown in Figure 4B. The maximum change in Coulomb stress is taken from the point on the ITSC where Coulomb stress reaches a maximum value. The results shown are for calculations assuming a tapered slip distribution along the source earthquake.

In the second scenario (Fig. 6), for $M_W \geq 5.0$, a source earthquake with relatively small *d* is calculated to cause significant Coulomb static stress increases on ITSC-parallel secondary normal faults. Such Coulomb stress changes correspond to a decrease in normal confining pressure across the ITSC axis, which may result in triggering of normal-faulting earthquakes or magmatic diking events along the ITSCs. The predicted Coulomb stress changes on secondary normal faults along the ITSC are a strong function of the location of the source earthquake. For example, if $M_w = 6.0$ and *d* is increased from 5 to 10 km, the calculated $\|\Delta\sigma_f\|$ decreases from 2.5 bar to 0.5 bar.

EXAMPLES OF POSSIBLE STRESS INTERACTION

Hydroacoustic monitoring of the East Pacific Rise (Fox et al., 2001) has allowed us to investigate several moderate-sized earthquakes to determine the role of transform segmentation in earthquake processes. Here, we have chosen one $M_W = 5.7$ teleseismically recorded earthquake that occurred in April 2001 along the S3 segment of the Siqueiros transform fault, which appears to have triggered seismicity on the S2 segment as well as on the ITSC SB (Fig. 7). Coulomb stress models were calculated using the source earthquake focal mechanism recorded in the Harvard CMT catalog, and the earthquake source location was taken from the hydroacoustic earthquake catalog.

The main shock ruptured the 24 km long S3 fault segment ~10 km from its intersection with the 8 km long ITSC SB. Approximately 170 aftershocks were recorded hydroacoustically within 24 h and 50 km of the epicenter of the main shock. The first 45 aftershocks (Fig. 7C) occurred along the fault segment S3 within 10 h of the main shock, and were spatially truncated by the ITSCs SB and SC. These aftershock locations correspond well with areas of predicted static stress increase along the source fault and on secondary strike-slip receiver faults along segment S3. Furthermore, the termination of the aftershocks east of the source fault at ITSC SC agrees with predicted estimates for segment interaction.

The subsequent 125 aftershocks (Fig. 7D) occurred on ITSC SB and the eastern end of the adjacent fault segment S2. The static stress models assuming transform-parallel strike-slip receiver faults do not predict this pattern of seismicity (Fig. 7C). Geologic interpretations of the Siqueiros transform by Fornari et al. (1989) indicate several ITSC-parallel faults flanking ITSC SB to the east, west, and north (Fig. 7B). As the latter 125 aftershock locations correspond well with areas of increased Coulomb stress for normal receiver faults, we hypothesize that these aftershocks might be associated with triggered seismicity on the normal faults mapped by Fornari et al. (1989). The ITSC-parallel tectonic fabric was created by ITSCs SA and SB, which appear to have slow-spreading ridge morphology (Fornari et al., 1989); this may account for the development of seismically active normal faults. Another possibility is that these aftershocks may reflect a diking event near ITSC SB resulting from main-shock-triggered decreases in confining pressure. Dynamic stress changes might also trigger aftershocks but are difficult to evaluate due to the lack of detailed main-shock rupture models.

CONCLUSIONS

Detailed analysis of earthquakes on transform systems at the East Pacific Rise suggests that segmentation geometry plays an important role in how slip is accommodated at fast-slipping oceanic transforms. Results of Coulomb stress models suggest that the length of the ITSC that offsets two transform fault strands will determine whether the adjacent fault segments will interact by static stress transfer. If the ITSC is sufficiently long, the adjacent segments will be decoupled and behave independently of each other. This is particularly important in studies of earthquakes at oceanic transforms, since a long oceanic transform system could be composed of several decoupled fault segments. Moreover, we illustrate that the thermal effect of ITSCs may reduce the thickness of the brittle layer, thus decreasing the potential rupture area and the maximum seismic moment of an oceanic transform fault system. Finally, we suggest that transform earthquakes may have the po-

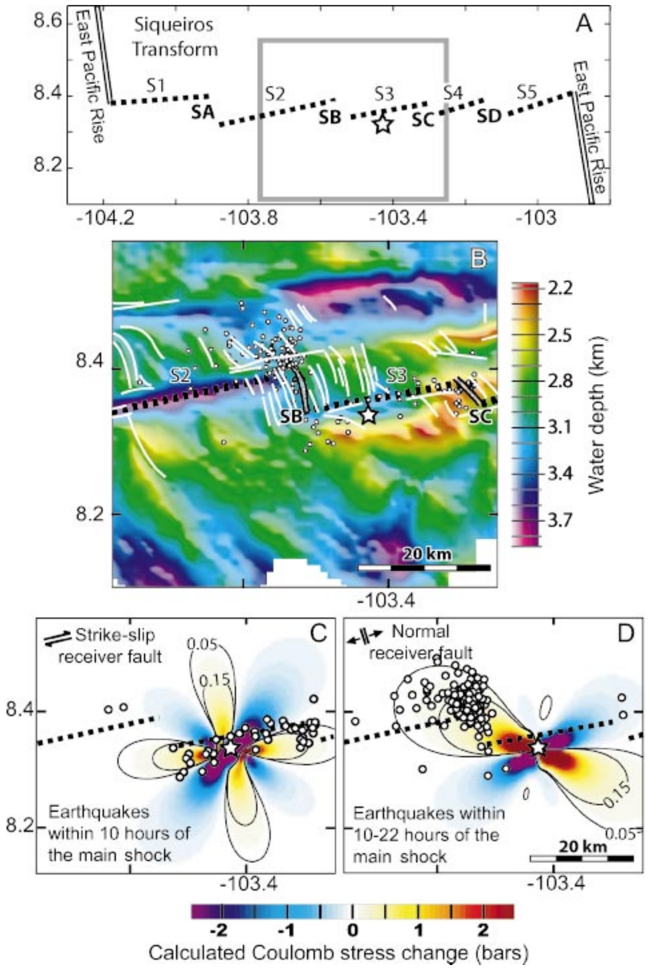

Figure 7. Coulomb stress models for a teleseismically recorded earthquake (M_w = 5.7, 26 April 2001) on the Siqueiros transform system. Earthquake location is shown by white star on each panel. A: Location map shows the segmentation geometry of Siqueiros. Outlined region indicates area investigated in B, C, and D. B: Bathymetric map overlain by the geologic interpretations (thin white lines) of Fornari et al. (1989). White circles indicate the locations of the 170 aftershocks. C: Calculated Coulomb static stress changes on secondary strike-slip receiver faults with the same dip, strike, and rake as the source earthquake. Source fault parameters from Harvard CMT focal mechanism: strike = 263°, dip = 81°, and scalar moment = 4.49 × 10^{24} dyne-cm. We assume rupture length = 5 km, width = 5 km, and slip = 0.36 m. We used a tapered slip distribution, and stresses were sampled on a horizontal plane at a depth of 2 km. Fox et al. (2001) estimate a lower threshold for earthquakes recorded within the hydrophone array of M_b = 1.0–1.8. The first 45 aftershocks (shown as white circles) occurred within ten hours of the main shock and fall along fault segment S3. The 0.15 bar and 0.05 bar contours are shown as solid black lines. We observe that ~31% of the first 45 aftershocks occurred in regions with stress increases ≥0.15 bar, and ~56% in areas with stress increases ≥0.05 bar. D: Calculated Coulomb static stress changes on secondary normal faults dipping 60° and parallel to the ITSC SB. The later 125 aftershocks (shown as white circles) correspond well with predictions of increased normal stress, thus suggesting that they might be associated with normal receiver faults. We observe that ~63% of the latter 125 aftershocks occurred in regions with stress increases ≥0.15 bar, and ~90% occurred in areas with stress increases ≥0.05 bar.

tential to trigger seismicity on secondary normal faults flanking ITSCs.

ACKNOWLEDGMENTS

This work was supported by an NSF (National Science Foundation) Graduate Research Fellowship (Gregg), NSF grant OCE-0221386 (Smith and Lin), and the Woods Hole Oceanographic Institution Deep Ocean Exploration Institute (Lin). We are grateful for helpful discussions with C. Williams, M. Behn, M. Boettcher, J. Cann, D. Fornari, D. Forsyth, J. McGuire, H. Schouten, and the WHOI geophysics group, and to D. Bohnenstiehl, E.A. Okal, and S. Toda for constructive and insightful reviews.

REFERENCES CITED

Abercrombie, R.E., and Ekstrom, G., 2001, Earthquake slip on oceanic transform faults: Nature, v. 410, p. 74–77.

Boettcher, M.S., and Jordan, T.H., 2004, Earthquake scaling relations for mid-ocean ridge transform faults: Journal of Geophysical Research—Solid Earth, v. 109, p. B12, doi: 10.1029/2004JB003110.

Bohnenstiehl, D.R., Tolstoy, M., Dziak, R.P., Fox, C.G., and Smith, D.K., 2002, Aftershock sequences in the mid-ocean ridge environment: An analysis using hydroacoustic data: Tectonophysics, v. 354, p. 49–70.

Bohnenstiehl, D.R., Tolstoy, M., and Chapp, E., 2004, Breaking into the plate: A 7.6 Mw fracture-zone earthquake adjacent to the Central Indian Ridge: Geophysical Research Letters, v. 31, p. B2, doi: 10.1029/2003GL018981.

Canales, J.P., Detrick, R., Toomey, D.R., and Wilcock, S.D., 2003, Segment-scale variations in the crustal structure of 150–300 kyr old fast spreading oceanic crust (East Pacific Rise, 8°15′ N–10°5′ N) from wide-angle seismic refraction profiles: Geophysical Journal International, v. 152, p. 766–794.

Dziak, R.P., Fox, C.G., and Embley, R.W., 1991, Relationship between seismicity and geologic structure of the Blanco transform zone: Marine Geophysical Researches, v. 13, p. 203–208.

Fornari, D.J., Gallo, D.G., Edwards, M.H., Madsen, J.A., Perfit, M.R., and Shor, A.N., 1989, Structure and topography of the Siqueiros transform-fault system—Evidence for the development of intra-transform spreading centers: Marine Geophysical Researches, v. 11, p. 263–299.

Forsyth, D.W., Yang, Y.J., Mangriotis, M.D., and Shen, Y., 2003, Coupled seismic slip on adjacent oceanic transform faults: Geophysical Research Letters, v. 30, doi: 10.1029/2002GL016454.

Fox, C.G., Matsumoto, H., and Lau, T.-K.A., 2001, Monitoring Pacific Ocean seismicity from an autonomous hydrophone array: Journal of Geophysical Research, v. 106, p. 4183–4206.

Goff, J.A., Fornari, D.J., Cochran, J.R., Keeley, C., and Malinverno, A., 1993, Wilkes transform system and nannoplate: Geology, v. 21, p. 623–626.

Harris, R.A., and Day, S.M., 1993, Dynamics of fault interaction—Parallel strike-slip faults: Journal of Geophysical Research—Solid Earth, v. 98, p. 4461–4472.

Hekinian, R., Bideau, D., Cannat, M., Francheteau, J., and Hebert, R., 1992, Volcanic activity and crust mantle exposure in the ultrafast Garrett transform fault near 13-degrees-28s in the Pacific: Earth and Planetary Science Letters, v. 108, p. 259–275.

King, G.C.P., Stein, R.S., and Lin, J., 1994, Static stress changes and the triggering of earthquakes: Bulletin of the Seismological Society of America, v. 84, p. 935–953.

Lonsdale, P., 1989, Segmentation of the Pacific-Nazca Spreading Center, 1° N–20° S: Journal of Geophysical Research, v. 94, p. 12,197–12,225.

McGuire, J.J., Jordan, T.H., and Lin, J., 2002, Complexities of transform boundaries in the oceans, *in* Stein, S., and Freymueller, J., eds., Plate boundary zones, volume 30: Washington, D.C., American Geophysical Union, p. 425.

McKenzie, D.P., 1969, Speculations on the consequences and causes of plate motions: Geophysical Journal of the Royal Astronomical Society, v. 18, p. 1–32.

Menard, H.W., and Atwater, T., 1969, Origin of fracture zone topography: Nature, v. 222, p. 1037–1040.

Perfit, M.R., Fornari, D.J., Ridley, W.I., Kirk, P.D., Casey, J., Kastens, K.A., Reynolds, J.R., Edwards, M., Desonie, D., Shuster, R., and Paradis, S., 1996, Recent volcanism in the Siqueiros transform fault: Picritic basalts and implications for MORB magma genesis: Earth and Planetary Science Letters, v. 141, p. 91–108.

Pockalny, R.A., 1997, Evidence of transpression along the Clipperton transform: Implications for processes of plate boundary reorganization: Earth and Planetary Science Letters, v. 146, p. 449–464.

Pockalny, R.A., Fox, P.J., Fornari, D.J., Macdonald, K.C., and Perfit, M.R., 1997, Tectonic reconstruction of the Clipperton and Siqueiros fracture zones: Evidence and consequences of plate motion change for the last 3 Myr: Journal of Geophysical Research—Solid Earth, v. 102, p. 3167–3181.

Searle, R.C., 1983, Multiple, closely spaced transform faults in fast-slipping fracture zones: Geology, v. 11, p. 607–610.

Stein, S., and Wysession, M., 2003, An introduction to seismology, earthquakes, and earth structure: Malden, Massachusetts, Blackwell Publishing, 498 p.

Toda, S., and Stein, R.S., 2000, Did stress triggering cause the large off-fault aftershocks of the 25 March 1998 Mw = 8.1 Antarctic plate earthquake?: Geophysical Research Letters, v. 27, p. 2301–2304.

Toda, S., Stein, R.S., Reasenberg, P.A., Dieterich, J.H., and Yoshida, A., 1998, Stress transferred by the 1995 Mw = 6.9 Kobe, Japan, shock: Effect on aftershocks and future earthquake probabilities: Journal of Geophysical Research—Solid Earth, v. 103, p. 24,543–24,565.

Manuscript received 26 August 2005
Revised manuscript received 21 November 2005
Manuscript accepted 22 November 2005

Printed in USA